8-20-2007

Chemical compositions at Mars landing sites subject to Mars Odyssey Gamma Ray Spectrometer constraints

Suniti Karunatillake
Cornell University

John M. Keller
Cal Poly San Luis Obispo

Steven W. Squyres
Cornell University

William V. Boynton
The University of Arizona

Johannes Brückner
Max Planck Institute for Chemistry

See next page for additional authors

Recommended Citation

Karunatillake, S., Keller, J., Squyres, S., Boynton, W., Brückner, J., Janes, D., Gasnault, O., & Newsom, H. (2007). Chemical compositions at Mars landing sites subject to Mars Odyssey Gamma Ray Spectrometer constraints. *Journal of Geophysical Research E: Planets, 112* (8) https://doi.org/10.1029/2006JE002859

Chemical compositions at Mars landing sites subject to Mars Odyssey Gamma Ray Spectrometer constraints

Suniti Karunatillake,[1] John M. Keller,[2] Steven W. Squyres,[1] William V. Boynton,[3] Johannes Brückner,[4] Daniel M. Janes,[3] Olivier Gasnault,[5] and Horton E. Newsom[6]

Received 11 November 2006; revised 19 March 2007; accepted 11 May 2007; published 2 August 2007.

[1] The Mars Odyssey Gamma Ray Spectrometer (GRS) is the first instrument suite to return elemental abundances throughout the midlatitudes of Mars. Concentrations of Cl, Fe, H, K, Si, and Th have been determined to tens of centimeter depths as mass fractions with reasonable confidence. Comparing such data with, or normalizing them to, in situ compositional data is difficult due to issues such as dramatic differences in spatial resolution; difficulties in convolving densities, abundances, and compositions of different regolith components; and a limited number of elements observed in common. We address these concerns in the context of the GRS, using Si at Pathfinder to normalize remote data. In addition, we determine representative in situ compositions for Spirit (both with and without Columbia Hills rocks), Opportunity, and Viking 1 landing sites using GRS-derived H content to hydrate the soil component. Our estimate of the Si mass fraction at Pathfinder, with 13% areal fraction of rocks, is 21%. The composition of major elements, such as Si and Fe, is similar across the four landing sites, while minor elements show significant variability. Areal dominance of soil at all four landing sites causes representative compositions to be driven by the soil component, while proportionally large uncertainties of bulk densities dominate the net uncertainties. GRS compositional determinations compare favorably with the in situ estimates for Cl and K, and for Si by virtue of the normalization. However, the GRS-determined Fe content at each landing site is consistently higher than the in situ value.

Citation: Karunatillake, S., J. M. Keller, S. W. Squyres, W. V. Boynton, J. Brückner, D. M. Janes, O. Gasnault, and H. E. Newsom (2007), Chemical compositions at Mars landing sites subject to Mars Odyssey Gamma Ray Spectrometer constraints, *J. Geophys. Res.*, *112*, E08S90, doi:10.1029/2006JE002859.

1. Introduction

[2] Mars Odyssey is the first Mars mission to provide elemental concentrations (as mass fractions) of global extent. These data have been generated with the Gamma Ray Spectrometer (GRS) instrument suite, which consists of the Gamma Subsystem (GS), Neutron Spectrometer (NS), and the High Energy Neutron Detector (HEND). Our discussion focuses on the GS. It consists of a passively cooled, n-type, reverse biased, high-purity Ge detector mounted on a 6m boom [*Boynton et al.*, 2004]. The boom and detector mounts are relatively free of geochemically significant elements in order to minimize interference from spacecraft components. At present, the GS determination methods have provided mass fraction data of global extent for the elements Cl, Fe, H, K, Si, and Th with reasonable uncertainties (W. V. Boynton et al., Concentration of H, Si, Cl, K, Fe, and Th in the low-latitude and midlatitude regions of Mars, submitted to *Journal of Geophysical Research*, 2006; hereinafter referred to as Boynton et al., submitted manuscript, 2006).

[3] In analyzing the GS data, a model composition is used to predict expected γ spectral peak intensities for each element subject to atmospheric corrections. The ratio of expected to observed intensities enables scaling of the model composition to represent the actual surface composition. Intermediate steps and assumptions therein introduce the potential for systematic errors, the presence or absence of which may be verified by comparing remotely determined elemental mass fractions with corresponding in situ values. Instruments similar to the Mars Odyssey GS (i.e., Ge based) are already en route to orbit Mercury

[1]Department of Astronomy, Cornell University, Ithaca, New York, USA.
[2]Physics Department, California Polytechnic State University, San Luis Obispo, California, USA.
[3]Lunar and Planetary Laboratory, University of Arizona, Tucson, Arizona, USA.
[4]Abteilung Geochemie, Max-Planck-Institut für Chemie, Mainz, Germany.
[5]Centre d'Etude Spatiale des Rayonnements/Centre National de la Recherche Scientifique/Université Paul Sabatier Toulouse, Toulouse, France.
[6]Institute of Meteoritics and Department of Earth and Planetary Sciences, University of New Mexico, Albuquerque, New Mexico, USA.

0148-0227/07/2006JE002859

[e.g., *McNutt et al.*, 2006] and planned for the Moon [e.g., *Kobayashi et al.*, 2005]. The future may hold similar missions to other solar system bodies and surface missions as well. Consequently, an effective approach to compare and normalize remote data with in situ estimates of a representative regolith composition could be useful even beyond Mars. In essence, such comparisons act as ''reality checks'' for remote observations, making the computation of representative in situ compositions a primary goal of our discussion.

[4] As described below, the effective instrumental spatial resolution of the GS is $\approx 3.7^{\circ}(\approx 220$ km) arc radius. In situ measurements at landing sites, on the other hand, involve samples of only centimeter and tens of centimeter spatial extent. Furthermore, lateral spacing of samples is only on the order of kilometers even for the Mars Exploration Rover (MER) mission, the most mobile mission to date. Additional concerns include dramatic differences in the sampling depths between remote instruments (the GS, for example) and surface instruments (the Pathfinder Alpha Proton X-ray Spectrometer, for example), a limited set of elements observed in common between them, and difficulties in convolving bulk densities and areal fractions of different regolith components with their compositions.

[5] Given the underlying issues, is it reasonable to compare the GS data with in situ data? In spite of all the caveats, there is a correspondence between these data sets in that the γ photons are produced in the upper few tens of centimeters of the Martian surface, which includes the surficial materials investigated by the landers and rovers. Furthermore, the nature of surficial material at the landing sites can be extrapolated to the GS spatial resolution scales with remote sensing data such as thermal inertia (sensitive to thermophysical properties of the upper surface such as thermal conductivity, bulk density, and heat capacity), mineralogic information [e.g., *Bibring et al.*, 2006b], and future visual observations at fine spatial resolution [cf. *Mustard and Cooper*, 2005; *Bibring et al.*, 2006a; *Shkuratov et al.*, 2005]. However, the massive difference in spatial resolution implicitly applies representative in situ compositions over GS footprint spatial scales whenever the GS data are compared or normalized with in situ values. We address this issue by using a weighted mean of rock and soil component compositions at landing sites, considered the ''ground truth'' composition.

[6] GS estimates of mass fractions of most elements are from intensities of γ spectral peaks above the continuum from scatter and capture neutron-nuclear reactions. The rates of these two reaction types, particularly capture, are strongly affected by the energy distribution of neutrons in the regolith. Presence of neutron moderators such as H at elevated concentrations can dramatically alter the neutron energy distribution, consequently affecting γ spectral estimates of elemental abundances. At present, these effects have not been modeled accurately for the extreme latitudes where H is compositionally layered as buried H_2O ice. Therefore the GS global data sets are constrained to the midlatitudes of Mars as delineated with a mask that excludes the polar regions where the H content begins to increase rapidly. However, data are available at the extreme latitudes for the radiogenic elements K and Th, since their γ photon production is independent of neutrons (Boynton et al., submitted manuscript, 2006).

[7] Elemental mass fractions determined with the GS are spatially binned on a uniform latitude-longitude grid, typically at $5^{\circ} \times 5^{\circ}$ resolution. Since the composition is estimated with the relative intensities of spectral peaks, only mass fractions, not absolute masses, of elements and oxides are estimated directly. This is different from wet chemical analysis of terrestrial rocks, for example, where ideally the total mass of all elements present must equal the known mass of the sample. In this case the oxidation states of important elements such as Fe may be determined directly. Other types of analyses, such as electron induced X-ray microanalysis (e.g., electron microprobe analysis at the micron scale), and remote and in situ spectral observations do not allow such rigor, and generally require reasonable oxidation states and absence of X-Ray invisible elements/minerals to be assumed for mass fraction normalization, as done by missions involving Alpha Particle X-Ray Spectrometers (APXS) of the Mars Exploration Rovers (MERs) [e.g., *Gellert et al.*, 2006], Alpha Proton X-Ray Spectrometer (APXS) of the Mars Pathfinder Sojourner rover [*Rieder et al.*, 1997], and X-Ray Fluorescence Spectrometers (XRFS) of the Viking Landers [*Clark et al.*, 1977]. Nevertheless, Mössbauer spectrometers enable the MER mission to determine Fe oxidation states.

[8] Where systematic differences between in situ and remote compositions are evident it is possible to normalize the remote data with in situ values. Insufficient information, on the galactic cosmic ray (GCR) flux, neutron energy distribution, and γ photon production factors [*Evans et al.*, 2006; *Masarik and Reedy*, 1996] to rigorously model all nonlinear relationships between composition and γ photon production necessitates this normalization for the GS. Abundances of radiogenic elements such as K and Th are unaffected by such issues and do not require normalization with in situ measurements.

[9] Normalization with in situ data would be reasonable only for elements that do not show much variability in mass fractions across landing sites. As such, Si, the most abundant element that is in situ and GS detectable, is the best choice for the GS normalization. An additional benefit of normalizing Si is that it has both capture and scatter derived γ peaks (refer to the work of *Evans et al.* [2006] for identification of individual peaks), while Cl, Fe, and H are primarily estimated with capture peaks. As discussed in section 2, the relationship between the normalized scatter-derived Si concentration and that derived via capture can indirectly resolve issues with capture-derived elemental concentrations. Given the importance of normalization to an in situ result, selecting a suitable value for the Si normalization is also a key goal of our work.

[10] We calculate representative in situ compositions at the Pathfinder Sojourner (at Ares Vallis), Spirit (at Gusev crater), Opportunity (at Meridiani Planum), and Viking 1 (at Chryse Planitia) landing sites. The Viking 2 landing site is excluded, given its proximity to the extreme latitude regions with elevated H and consequent exclusion from reported GS results.

2. Key GS Data Processing Steps

[11] There are numerous intermediate steps to generating mass fractions with the GS, which are discussed in detail by

Boynton et al. (submitted manuscript 2006), *Evans et al.* [2006], and *Kim et al.* [2006b]. We focus only on those immediately relevant for the comparison between remote and in situ compositions. Key among them, in the general order in which they are applied, are: model composition grid, scatter corrections, spatial filter, normalization of Si mass fractions (w(Si)) to an in situ value, and capture corrections.

2.1. Model Composition Grid and Instrumental Spatial Resolution

[12] The model composition grid is the starting point for GS determination of the Martian regolith composition. The grid consists of $0.5^\circ \times 0.5^\circ$ cells, with each assumed to be compositionally homogeneous at the few tens of centimeter sampling depth scale of the GS (the model composition is described by Boynton et al. (submitted manuscript, 2006)). The γ photon count rates in orbit due to each cell and a given nuclear reaction may be predicted with neutron production simulations, stochastic parameters, regolith attenuation coefficients, and atmospheric attenuation coefficients [*Evans et al.*, 2006; *Kim et al.*, 2006b; Boynton et al., submitted manuscript, 2006]. Even though the Martian atmosphere acts as a weak collimator, since the GS is an uncollimated instrument, it receives γ photons from limb to limb at the nominal 400km altitude mapping orbit [e.g., *Boynton et al.*, 2004]. Therefore the set of cells within which >99% of the signal originates is used for predictive modeling, corresponding to a nadir-centered signal contribution region (SCR) of $\approx 17^\circ$ (i.e., 1000 km) arc radius [*Kim et al.*, 2006b].

[13] For a given nuclear reaction of each element, the ratio of predicted γ photon counts to the observed is computed within the SCR. This ratio scales the model composition, yielding an estimate of the actual composition. The estimated composition is assigned to the cell at nadir, and the process repeated for each cell of the $0.5^\circ \times 0.5^\circ$ grid. Such a fine grid is appropriate for data processing and display, but does not represent the actual footprint of the GS, which is defined by the set of cells that contribute more than 50% of the signal. While dependent on photon energies, the typical footprint is $\approx$440 km, corresponding to $\approx 7.4^\circ$ arc diameter [e.g., *Boynton et al.*, 2004; Boynton et al., submitted manuscript, 2006].

[14] When photons of differing energies are emitted by a single element, a weighted mean of corresponding mass fractions is generally used to represent the true composition of the element (Boynton et al., submitted manuscript, 2006). The signal-to-noise ratio is maximized by the use of cumulative spectra over durations of one to two Martian years called epochs (we use the epoch from 08 Jun 2002 to 02 Apr 2005). The large number of cells within each SCR and the use of epochal γ spectra yield statistically rigorous uncertainties that are primarily functions of counting statistics and smaller than model composition uncertainties [*Evans et al.*, 2006; Boynton et al., submitted manuscript, 2006].

[15] The regolith model may introduce systematic errors for all elements, while the model composition may do so for elements determined with capture or scatter processes. The GS regolith model for the midlatitudes assumes compositional homogeneity at GS sampling depths. It also assumes lateral compositional homogeneity within each cell. Significant deviations from lateral homogeneity have the potential of seriously weakening the accuracy of GS compositional estimates, as would the presence of compositional layering [e.g., *Squyres and Evans*, 1992]. We consider such deviations and explain what we classify as rocks and other material in section 3.

2.2. Scatter Corrections, Spatial Filter, and Effective Spatial Resolution

[16] Scatter corrections constitute another important step in the reduction of GS data. Si mass fractions derived from the 1779 k eV γ flux are subject to the scatter corrections, increasing the initial Si estimates by $\approx \times 3$ on average. These correction factors, which account for variations in the fast neutron flux driven mainly by Fe and H content in the regolith, precede the spatial filter application, Si normalization to an in situ value, and capture correction determination (Boynton et al., submitted manuscript, 2006).

[17] The third processing step, spatial filter application, is important in the context of instrument detection efficiency and resolution. The choice of a gamma ray spectrometer type is a trade off between the high efficiency of scintillators and the high energy resolution of solid state detectors [*Metzger and Drake*, 1990; *Pirard et al.*, 2005]. The latter option was appropriate for the Mars Odyssey GS, where the ability to resolve and identify many of the lines that characterize the Martian spectrum optimized the science return [*Boynton et al.*, 2004; Boynton et al., submitted manuscript, 2006]. Nevertheless, GS data have low signal-to-noise ratios at fine spatial scale. This concern is addressed by first smoothing with a constant arc radius mean filter. The mean filter is applied simultaneously, not iteratively, on a $0.5^\circ \times 0.5^\circ$ grid with the arithmetic mean of values within the filter window assigned to the central cell. Boynton et al. (submitted manuscript, 2006) discuss and illustrate the scatter of values before and after the smoothing.

[18] To first order, the filter radius is greater for elements with smaller signal-to-noise ratios. For nonradiogenic elements in particular, the spatial filter is applied at several processing steps (Boynton et al., submitted manuscript, 2006). The filter arc radii for different elements at the final processing steps are: 5° for K; 10° for Cl, Fe, H, and Th; and 15° for Si. An unfortunate outcome of filtering is the increase in spatial uncertainty in the form of spatial autocorrelation. As the mutual dependence of spatially adjacent data, spatial autocorrelation leads to fewer degrees of freedom than the number of data [e.g., *Haining*, 2003, pp. 273–324]. Subsequent to the filter application, the data are binned on fairly coarse latitude-longitude grids, typically at $5^\circ \times 5^\circ$. Rebinning further increases the signal-to-noise ratio and provides the necessary oversampling to account for the difference in shape between the response function of the GS, which is circular, and of cells, which are rectangular. However, since the filter window is much larger than an individual $5^\circ \times 5^\circ$ spatial bin, spatial autocorrelation is aggravated in the GS data. Nevertheless, the filter enables a significant increase in numerical precision as evident in relative root-mean-square uncertainties of 10% for Cl, 8% for Fe, 11% for H, 7% for K, 2% for Si, and 10% for Th.

[19] A combined effect of the spacecraft footprint, the SCR, and the spatial filter is a dramatic difference in spatial resolution between the GS and in situ instruments. This difference necessitates careful selection of compositional attributes from in situ missions for comparison with and normalization of the GS data. It is particularly important as the GS is insensitive to the substantial variability at small lateral spatial scales, in composition, density, and texture as seen by the Viking, Pathfinder, and MER missions.

2.3. Si Normalization, Capture Corrections, and Feedback Effects

[20] As described earlier, we select only one element, Si, for the normalization of GS data. The normalization is achieved in several steps. First, the scatter-derived 1779 k eV γ photons from Si are used to estimate w(Si) subject to the scatter corrections. These mass fractions are then smoothed with the mean filter. Next, the filtered values are scaled by a constant so that the GS-derived w(Si) at the coordinates of a chosen landing site equals the representative in situ w(Si). For reasons discussed in section 6.4, we chose the Pathfinder landing site for the Si normalization.

[21] Capture corrections are subsequently determined as the ratio of the capture-derived w(Si) to the 1779 keV scatter-derived (also scatter corrected and normalized) w(Si) at each cell (e.g., Boynton et al., submitted manuscript, 2006). These ratios act as scaling factors for mass fractions of all capture-derived elements (Cl, Fe, and H) (Boynton et al., submitted manuscript, 2006), increasing initial estimates by $\approx\times 4$ on average. Such scaling is necessary to account for variations of the thermal neutron flux in the regolith due to the presence of neutron moderators, such as H, even at low concentrations (Boynton et al., submitted manuscript, 2006).

[22] A slight feedback effect exists between the scatter and capture correction steps, since Fe and H content, which are subject to the capture correction, affect the scatter correction. Furthermore, as described in section 5, we renormalize the calculated in situ composition to allow for the presence of GS-determined H, which in turn affects the Si normalization. However, these feedback effects among the scatter correction, capture correction, and Si normalization are so subtle that the relative variation in estimated elemental mass fractions during iterative processing was <0.1%.

3. Summary of the Technique

[23] As outlined in section 1, since we compute a weighted mean of in situ rock and soil compositions, it is important to classify regolith components into these two categories. Throughout our discussion, ''rocks'' generally refer to 10 cm scale and larger materials (e.g., fragments, breccia, and exposed outcrops) that have high thermal inertia, have areal fractions consistent with the Viking Infrared Thermal Mapper (IRTM) data [e.g., *Christensen*, 1986; *Golombek et al.*, 2005], and are immobile under current eolian conditions. The mean free path of neutrons is ≈10 cm [e.g., *Squyres and Evans*, 1992], ensuring that what we consider as rocks appear distinct to the GS. ''Soil'' refers to all other, typically unconsolidated, material including those sufficiently fine-grained to be mobilized by wind [e.g., *Banin et al.*, 1992; *Jerolmack et al.*, 2006]. Soil consequently encompasses a variety of regolith components identified at the five landing sites. Typical examples are: bedform armor, clasts, concretions, drift, dust, rocky fragments, sand, and soil [e.g., *Fergason et al.*, 2006; *Golombek et al.*, 2005; *Sullivan et al.*, 2005; *Yen et al.*, 2005].

[24] While our classification of the regolith into rocks and soil is very broad, it suits the GS data context, with the ≈440 km instrument footprint and upper few tens of centimeter sampling depth as described in section 2 (e.g., Boynton et al., submitted manuscript, 2006). For example, the GS would be insensitive to the variability of rock areal fraction by factors of two to four [e.g., *Squyres et al.*, 2004b] as observed in the km scale traverse of Spirit. Satisfactory agreement between average in situ estimates and IRTM orbital estimates of the areal fraction of rocks further support our simple classification [e.g., *Golombek et al.*, 2005]. However, our rock size threshold assigns smaller rock fragments to the soil component, potentially making the areal fraction we assign to rocks less than their in situ value. In addition, since the daily temperature variations do not penetrate very far into rock, and less into soil, even a thin (>1 cm) soil layer can conceal rocks from the IRTM and lead to an underestimation of the rock abundance.

[25] For a regolith with two key components, rock and soil materials, distributed as a homogenous mixture within a sample volume, we may compute the representative mass fraction of an element or oxide as

$$C_{\mathrm{m}} = \frac{c_{\mathrm{r}} A_{\mathrm{r}} \rho_{\mathrm{r}} + c_{\mathrm{s}}(1 - A_{\mathrm{r}})\rho_{\mathrm{s}}}{A_{\mathrm{r}} \rho_{\mathrm{r}} + (1 - A_{\mathrm{r}})\rho_{\mathrm{s}}} \tag{1}$$

with C_{m} the representative in situ concentration of the element (or oxide) as a mass fraction, A_{r} the areal fraction of rocks, ρ_{r} the density of rocks, ρ_{s} the density of soil, c_{r} the mass fraction of the element (or oxide) in rocks, and c_{s} the mass fraction of the element (or oxide) in soil. Uncertainties are propagated for C_{m} and all other computed values with the standard formula [e.g., *Young*, 1962, pp. 96–101]:

$$s_{\mathrm{m}} = \sqrt{\sum_i \left|\frac{\partial f}{\partial x_i}\right|^2 s^2_{m,x_i}} \tag{2}$$

where x_i is the ith variable of the function f, s_{m,x_i} the standard error (i.e., net uncertainty defining 68% statistical confidence under normality assumptions) of x_i, and s_{m} the standard error of the function. Therefore, under Gaussian assumptions, f would be 68% probable to be within $1s_{\mathrm{m}}$. Following the notation within companion papers of the Mars Odyssey Special Issue [e.g., *Karunatillake et al.*, 2006; *Keller et al.*, 2006b; *Taylor et al.*, 2006a; Boynton et al., submitted manuscript, 2006], we state uncertainties to $1s_{\mathrm{m}}$. In contrast, the MER team reports APXS data uncertainties to $2s_{\mathrm{m}}$ [e.g., *Gellert et al.*, 2006; *Rieder et al.*, 2004].

[26] For a given soil type at each MER site, we estimate c_{s} in equation (1) as the arithmetic mean ($\hat{\mu}$) of several samples identified in sections 6.2 and 6.3. The corresponding standard error ($s_{\mathrm{m},x_i} = s_{\mathrm{m},c_{\mathrm{s}}}$) for use in equation (2) is derived from the standard deviation $s =$

Table 1. Areal Fractions of Rock and Soil Components at the Landing Sites as Discussed in Section 4[a]

		Rock Areal Fraction	Soil Areal Fraction	
Lander/Rover	s_m	A_r	A_d	A_s
Opportunity		9	91	
Pathfinder		13	87	
Spirit	5	6	94	
Viking 1		13	18 ± 4.	66. ± 13.
Viking 2		16	30. ± 6.	54. ± 11.

[a]Areal fractions are in %. The reported relative areal fractions of "drift" (A_d) and "soil" (A_s) are used in equation (3). Note that the calculated composition at Opportunity assumes a rock-free surface as described in section 6.3.

$\sqrt{\frac{\sum_i (c_{s,i}-\hat{\mu})^2}{N-1}}$ as $s_{m,c_s} = \frac{s}{\sqrt{N}}$, where N is the number of samples and $c_{s,i}$ is the concentration in the ith sample [e.g., *Mandel*, 1964, pp. 35–41, 62–63, 106–110]. The alternative of computing the maximum likelihood mean and corresponding s_{m,c_s} using the reported uncertainties is less defensible in the rover context, since such samples generally present statistically inconsistent [e.g., *Taylor*, 1982, pp. 147–152] data even though they are spatially indistinct from the GS perspective. We similarly utilize the standard error of the arithmetic mean along with calibration uncertainties for Viking 1 data. In all other cases, we use the reported standard error as s_{m,x_i}, which is primarily driven by counting statistics for the GS data. In summary, the standard error of C_m is mostly a function of the following: (1) statistical uncertainties in rock and soil densities as described in section 4, (2) reported uncertainty in rock areal fraction (Table 1), (3) reported uncertainties of in situ element/oxide mass fractions (with the exception of MER soil data as described above), and (4) the standard error of GS-derived $w(H_2O)$ (Table 3 and section 5).

[27] A difficulty with equation (1) is that density, areal fraction, and element concentration measurements are not simultaneously available for a given landing site. In addition, equation (1) is valid only where the regolith is a homogenous mixture of rocks and soil across the γ photon sampling depth, which, as discussed in section 2, is also a primary assumption of all GS data sets. While this assumption may be roughly true for the Gusev, Pathfinder, and Viking landing ellipses [e.g., *Moore et al.*, 1977; *Golombek et al.*, 2005], Meridiani is a clear exception as noted in section 6.3. The effect of rock/soil mixing geometries on mass fraction estimation has been modeled before [e.g., *Squyres and Evans*, 1992]. Additional studies are underway to quantify these effects for rocks embedded in a soil matrix [e.g., *Kim et al.*, 2006a].

4. Bulk Densities and Areal Fractions

[28] An estimate of rock and soil bulk densities is key to evaluating equation (1). However, none of the in situ missions have been equipped with instruments to directly determine bulk densities. Consequently, the most reliable density estimates to date are from reasonable terrestrial analogues that utilize thermophysical, textural, and compositional information of the Martian regolith [e.g., *Fergason et al.*, 2006; *Grant et al.*, 2004]. While bulk densities of Martian rocks would be consistent with those of Shergottite-Nakhlite-Chassignite (SNC) meteorites, it is important to note that SNC meteorites may not be petrologically representative of the general Martian regolith [e.g., *McSween*, 1994, 2002].

[29] In the case of the MER, Rock Abrasion Tool (RAT) currents and Mössbauer contact plate forces provide additional estimates of rock and soil properties, respectively [e.g., *Arvidson et al.*, 2004a, 2004b; *Squyres et al.*, 2006a]. In addition, the Panoramic Cameras (Pancams) [e.g., *Farrand et al.*, 2006; *Bell et al.*, 2004] and Microscopic Imager (MI) [e.g., *Sullivan et al.*, 2005; *Cabrol et al.*, 2006; *Herkenhoff et al.*, 2006] yield detailed textural information. Overall, the MER mission has provided evidence of much greater variability in bulk properties than recognized on earlier missions [e.g., *Fergason et al.*, 2006]. Nevertheless, in the context of remote missions sensitive only to average physical properties at coarse spatial resolution, detailed modeling of in situ bulk densities is unlikely to yield useful insight. Therefore we utilize the Viking regolith property observations and corresponding terrestrial analogs as our primary sources of density information, supplemented with evidence for heterogeneity as observed by the MER mission.

[30] The density of "average" Martian rocks, considered physically analogous to terrestrial dense basalts [e.g., *Fergason et al.*, 2006; *McSween et al.*, 2004], is taken to be $(2.6 \pm 0.5) \times 10^3$ kg m^{-3} [*Moore et al.*, 1977; *Moore and Jakosky*, 1989; *Olhoeft and Johnson*, 1989]. To account for significant variability in rock bulk densities, we quote and substitute the standard deviation (s) instead of the standard error of ρ_r in $s_{m,x_i} = s_{m,\rho_r}$ of equation (2). Two soil components were identified at the Viking 1 site: "drift" with a density of $(1.15 \pm 0.15) \times 10^3$ kg m^{-3} and "blocky soil" with a density of $(1.6 \pm 0.4) \times 10^3$ kg m^{-3} [*Moore and Jakosky*, 1989]. While the near-field analysis by *Moore and Jakosky* [1989] identified only a "crusty to cloddy soil" with a density of $(1.4 \pm 0.2) \times 10^3$ kg m^{-3} at the Viking 2 site, the far-field analysis by *Moore and Keller* [1991] verified the presence of "drift" as well. Since soil densities at each site overlap within the uncertainties, we use their far-field areal fraction weighted mean as the density of the soil in equation (1). The mean density of the soil, ρ_s, may then be expressed as:

$$\rho_s = \frac{A_d \rho_d + A_s \rho_s}{A_d + A_s} \tag{3}$$

where d represents "drift" and s represents "soil" ("blocky" type at Viking 1 and "crusty to cloddy" type at Viking 2). The remaining symbols are analogous to those of equation (1), with the standard error of ρ_s obtained by substituting $f = \rho_s$ in equation (2).

[31] Since Viking 1 and 2 reported different relative areal fractions (Table 1) and densities for the "drift" and "soil" components, ρ_s differs slightly between the two soil proxies. For the Pathfinder and MER landing sites where density estimates have not been reported, the maximum-likelihood mean [e.g., *Mandel*, 1964, pp. 131–135] of the two, $(1.34 \pm 0.13) \times 10^3$ kg m^{-3}, was used as the mean density, ρ_s, of the soil component. This approximation is further justified by the favorable comparison of soil properties across Viking, Pathfinder, and MER landing sites [e.g., *Arvidson*

et al., 2004a]. On the other hand, ρ_s at the Viking 1 landing site was computed directly from equation (3) to be $(1.5 \pm 0.3) \times 10^3$ kg m^{-3}.

[32] In addition to the densities of the rock and soil components, equation (1) requires the areal fraction of rocks, A_r. As explained in section 3, we rely on the global rock areal fraction map at $1^\circ \times 1^\circ$ resolution generated with thermal inertia data from the IRTM [*Christensen*, 1986]. We compute the mean of rock areal fractions within a 15° arc radius circle, representative of the GS spatial filter and centered at the coordinates of each landing site: Viking 1 (22.27° latitude, −47.94° east longitude) [*Mayo et al.*, 1977], Pathfinder (19.13°, −33.22°) [*Golombek et al.*, 1999], Spirit (−14.57°, 175.47°) [*Squyres et al.*, 2004b], and Opportunity (−1.95°, −5.53°) [*Squyres et al.*, 2004a]. The absolute, not relative, uncertainty of each mean rock areal fraction is taken to be 5% [e.g., *Christensen*, 1986]. These are summarized in Table 1.

5. Oxidation and Hydration

[33] We compare compositions across landing sites while conforming with wet chemical analysis normalization of mass fractions at each site to unity. This requires the oxidation state of a given element to be the same across all landing sites for both rock and soil. Reported values satisfy this condition for most elements, with the exception of Fe and S. We adjust the oxidation states of these two elements in three steps. First, we stoichiometrically (atomic masses by *Loss* [2003]) convert reported oxide mass fractions of all elements into the unoxidized (i.e., elemental) mass fractions. Second, we convert the elemental mass fractions back into oxide mass fractions assigning the same oxidation state to a given element across all regolith components and landing sites. Third, we separately renormalize these mass fractions to unity for rock and soil.

[34] Only Pathfinder data needed the oxidation state adjustment for S, by converting rock composition from S to S^{6+}. The adjustment for Fe is much more complicated. To date, the MER Mössbauer spectrometer is the only instrument to measure in situ Fe oxidation states. While the MER data demonstrate significant variability in the molar fraction of Fe^{3+}, once the outcrop and hematitic soils in Meridiani and the Columbia Hills rocks in Gusev are excluded, the molar fractions are in rough agreement between the two sites [*Klingelhöfer et al.*, 2004; *Morris et al.*, 2004]. It is important to note however, that the Fe oxidation states observed in the Columbia Hills indicate much variability, with the molar fraction of Fe^{3+}, $\frac{Fe^{3+}}{Fe_{total}}$, varying from approximately 0.2 to 0.9 [*Morris et al.*, 2006a]. Columbia Hills rocks are also older than the plains rocks [e.g., *Squyres et al.*, 2006a], and may be comparable in age to the bedrock beyond the crater rim. While these concerns indicate that using a mean of Fe oxidation states observed across landing sites may be simplistic, as explained in section 7, its effect on the computed in situ composition is negligible due to the normalization of oxides. In contrast, a major systematic error could occur if Fe and/or S existed in sulfide or elemental form instead of as oxides.

[35] Since Fe oxidation states vary significantly between and within the only two sites where such data are available, we use the Gusev plains material to estimate a mean molar fraction of Fe^{3+} solely as a formalism. The arithmetic mean and standard deviation of the Fe^{3+} molar fraction of all measurements in the Gusev plains is 0.28 ± 0.01 [*Morris et al.*, 2004]. Consequently, we use a mean Fe oxidation state of +2.28 as the standard in all our representative in situ estimates. The renormalizations of reported compositions to $FeO_{1.14}$ and SO_3 preceded all other calculations.

[36] While GS measurements include w(H) (reported as stoichiometrically equivalent $w(H_2O)$), H content has not been directly determined in situ [*Rieder et al.*, 2003; *Gellert et al.*, 2006], with the exception of the Viking landers [e.g., *Anderson and Tice*, 1979]. We model the rock component to be devoid of H_2O, and propagate the GS-derived $w(H_2O)$ into the soil component. This is achieved by inverting equation (1):

$$c_s = \frac{C_{GS}\{A_r\rho_r + (1 - A_r)\rho_s\}}{(1 - A_r)\rho_s} \quad (4)$$

where c_s is the estimated in situ $w(H_2O)$ in soil, and C_{GS} the GS-derived $w(H_2O)$ at the landing site coordinates. C_{GS} values and corresponding standard errors are listed in Table 3, and we compute the standard error of c_s by substituting $f = c_s$ in equation (2). The in situ oxide and elemental mass fractions in soil are renormalized to $1 - c_s$ to allow for the presence of H_2O. In spite of exceptions [e.g., *Clark et al.*, 2005] discussed in section 6.3, assuming the rock component to be free of H_2O remains a reasonable approximation for the majority of landing sites. As a concluding step, we convert the representative in situ compositions, renormalized for both uniform oxidation states and the presence of H, into stoichiometrically equivalent elemental mass fractions.

[37] In general, C_{GS} values (Table 3) are consistent with in situ estimates of $w(H_2O)$ at Pathfinder, Spirit, and Viking 1. At pathfinder, the stoichiometric $w(H_2O)$ is ≈2% in soils and 0.1%−−4.3% in rocks as calculated via mass balance and subject to Fe and S oxidation state assumptions [*Foley et al.*, 2003]. The re-analysis of Viking 1 data indicated that the soil at Viking 1 may contain $w(H_2O)$ in the range 1.1%−−3.0% [*Anderson and Tice*, 1979]. Mineralogic modeling of H_2O content at Spirit is difficult due to the large mineralogic variability of regolith components that contain H. Nevertheless, current modeling tentatively suggests $w(H_2O)$ ≈0.7% as Goethite (α − FeOOH) in the most altered Gusev rocks [*Morris et al.*, 2006a] and $w(H_2O)$ < 11% as hydrated sulfates in subsurface soils [*Wang et al.*, 2006]. Furthermore, recently analyzed salt deposits in the Columbia Hills, such as Paso Robles, may contain much higher amounts of bound H_2O [e.g., *Lane et al.*, 2007; *Wang et al.*, 2007; J. R. Johnson et al., Mineralogic constraints on sulfur-rich soils from Pancam spectra at Gusev Crater, Mars, manuscript in preparation, 2007; A. Yen et al., Soil geochemistry with an emphasis on Paso Robles class materials, manuscript in preparation, 2007].

6. In Situ Specifics

[38] In spite of the generally similar methodology to estimate representative in situ compositions, some differences arise in the calculation details at different landing sites. These differences reflect the compositional diversity

on Mars and differences in instrumental capabilities. For example, the elemental composition of the Viking 1 landing site is not as well characterized as the others, since the XRFS had more limited elemental detection capabilities than the APXS used in subsequent missions. Moreover, the MER mission provides additional information due to a comprehensive suite of instruments and mobility.

[39] MER instruments are sensitive to geochemical variations at spatial scales vastly exceeding the sensitivities of remote (e.g., the GS) missions. For example, the MERs have revealed striking morphological, textural, and compositional variations [e.g., *Arvidson et al.*, 2006; *Cabrol et al.*, 2006; *Grotzinger et al.*, 2005] at centimeter to tens of centimeter scales with elemental and mineral detection instruments (the APXS [e.g., *Gellert et al.*, 2006], Miniature Thermal Emission Spectrometer (Mini-TES) [*Fergason et al.*, 2006], and Miniature Mössbauer Spectrometer (MIMOS II) [*Morris et al.*, 2006a]) and at sub-millimeter scales with the MI [e.g., *Herkenhoff et al.*, 2006]. As an additional complexity, Spirit has observed chronological variability, including the removal of a thin dust cover by dust devils [e.g., *Arvidson et al.*, 2006; *Greeley et al.*, 2005]. Consequently, while we use all the samples of earlier in situ missions, only a carefully selected subset of the MER data is used for remote comparisons.

6.1. Viking 1

[40] All Viking data may be used in representative in situ estimations since major compositional heterogeneities were inevident due to instrumental limitations and lack of mobility. The absence of rock compositional data poses a challenge at the Viking site. Given the general geological similarities and spatial proximity of the regolith at Viking 1 and Pathfinder, we address this by using the Pathfinder mean soil-free rock composition [*Wänke et al.*, 2001] as a proxy for the rock composition at Viking 1. However, the apparent geological similarities may conceal significant compositional differences, with the potential to invalidate our choice of a proxy rock composition. Nevertheless, relative to Pathfinder, rock compositions at either MER site are likely to be even more inappropriate as proxies to rock at Viking (see below).

[41] Besides the lack of rock analyses, the Viking 1 XRFS was also incapable of detecting Cr, Mn, Na, and P. Consistent with the approach by *McSween and Keil* [2000], for example, we account for this issue by normalizing Viking 1 rock and soil compositions to 97%, the net mass fraction of Pathfinder soil-free rock attributable to elements and oxides other than Na_2O, Cr_2O_3, MnO, and P_2O_5. Furthermore, the mean K content based on the work of *Clark et al.* [1982] is below the XRFS detection limit. We use the arithmetic mean of values reported by *Clark et al.* [1982] to estimate the Viking 1 soil composition.

6.2. Spirit

[42] We utilize the reported APXS data for Spirit [*Gellert et al.*, 2006]. The choice of a suitable rock composition in the context of the GS footprint is somewhat complicated at Gusev. The uncontaminated composition of rocks in the Gusev crater floor could be represented effectively by the APXS measurements following the second RAT application (RAT 2) on the plains rock "Humphrey" (Figure 1 and Table 2) [*Gellert et al.*, 2004]. However, rocks in the "Columbia" Hills are chemically altered, vary significantly in composition leading to at least five compositionally distinct classes, and are inferred to be geologically older (possibly Noachian) than the potentially Hesperian plains rocks [e.g., *Arvidson et al.*, 2006; *Cabrol et al.*, 2006; *Squyres et al.*, 2006a].

[43] While the Columbia Hills constitute <5% of the area within Gusev crater, the crater itself, with a diameter of ≈160 km [*Squyres et al.*, 2004b], accounts for only ≈13% of the GS footprint. The bedrock beyond the crater is more likely to be of a geological age comparable to the Columbia Hills than the Gusev plains. Consequently, using only Humphrey RAT 2 data to represent the rocks of Gusev may be more inappropriate than an areally weighted mean of Gusev plains and Columbia Hills rock compositions. We consider both options, as they reflect the complexity of Martian surface composition and the difficulty of selecting a particular composition to represent even a single location at the spatial scale of a GS footprint. Though found only as float, the composition of "Wishstone" class brushed and abraded rock (Figure 1 and Table 2) is used to represent the Columbia Hills rock composition as it has been fairly common in the Columbia Hills, and is similar in elemental composition to the "Watchtower" class of outcrop [*Squyres et al.*, 2006a; *Gellert et al.*, 2006].

[44] Compositional differences between the typical crater floor soils (sampled with the "Boroughs" and "Big Hole" trenches, Figure 1 and Table 2) and "hollows" (sampled with the "Road Cut" trench, Figure 1 and Table 2) complicate the choice of a representative soil composition at Gusev. As discussed for equations (1) and (2), we use four samples from Boroughs and Big Hole trenches to represent the typical soil, and two samples from the Road Cut trench to represent hollows soil. Hollows appear to be relatively young eolian infill of small impact craters, while the surrounding plains contain mature soil material [e.g., *Haskin et al.*, 2005; *Wang et al.*, 2006]. Furthermore, in spite of the ubiquity of hollows [*Golombek et al.*, 2006], plains soils are areally dominant along the rover traverse [*Arvidson et al.*, 2004a; *Grant et al.*, 2004]. In light of these issues, we compute a 9 to 1 ratio mean of plains to hollows as the representative composition of soil at Gusev, which is supported in part by areal evidence presented by *Golombek et al.* [2006].

[45] In spite of compositional complexities, trench data sampling up to ≈11cm deep in the making of Boroughs are much more relevant at GS sampling depth scales than any surface soil measurement. The MER trench campaigns were motivated primarily by this consideration [*Wang et al.*, 2006], and have revealed the presence of significant compositional layering at tens of centimeter depths [e.g., *Haskin et al.*, 2005; *Soderblom et al.*, 2004; *Wang et al.*, 2006]. This observation is not contradicted by the lack of evidence in GS data for Cl layering at large lateral spatial scales [*Keller et al.*, 2006a], since Br and Cl in particular have shown highly localized vertical variations at both Gusev [e.g., *Wang et al.*, 2006] and Meridiani [e.g., *Rieder et al.*, 2004].

6.3. Opportunity

[46] In contrast to Gusev and other landing sites, the surface at Meridiani consists of a layer of soil with variable

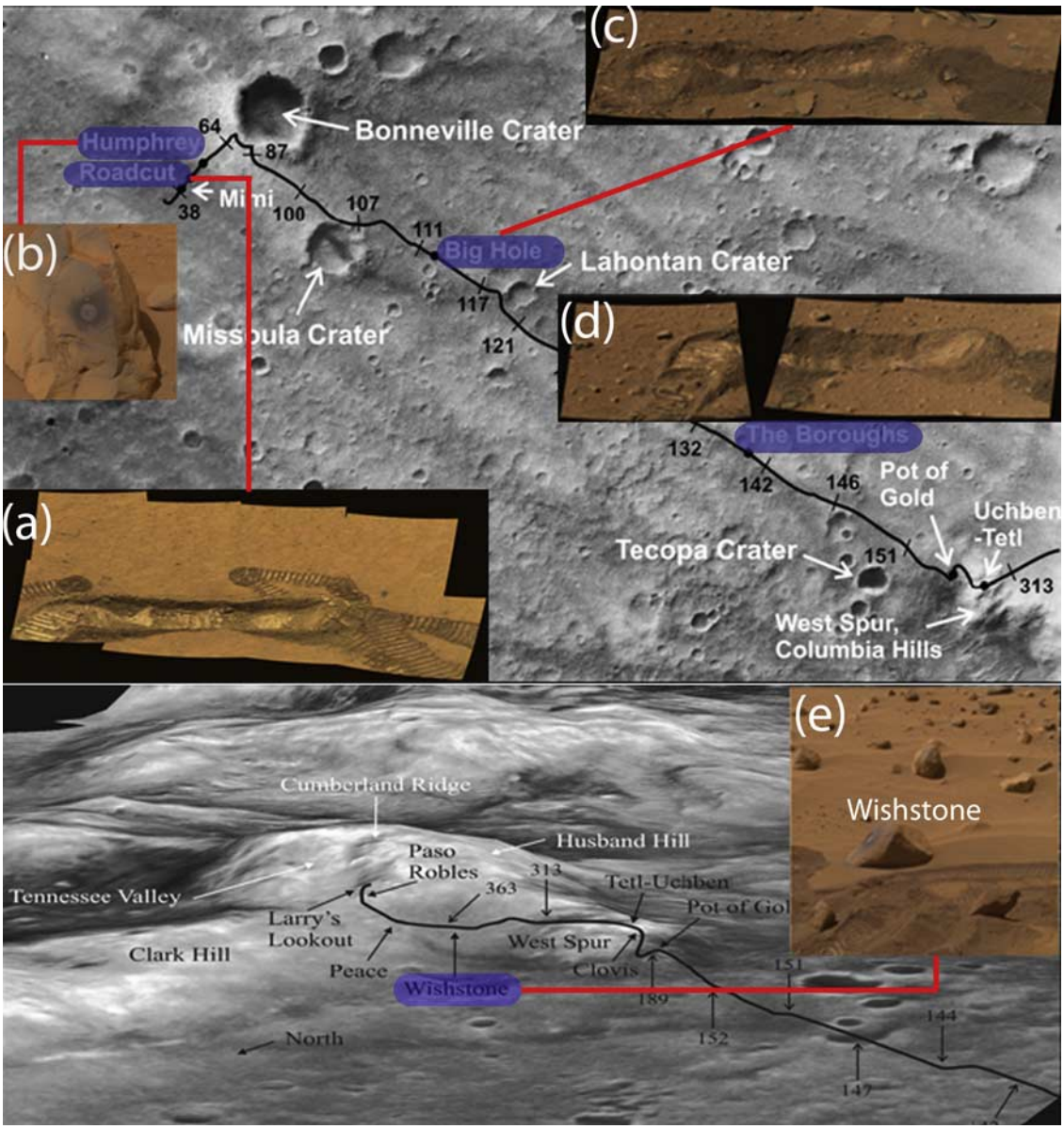

Figure 1. Images of rocks and trenches at Gusev that were used to obtain APXS data for our study as traverse map insets. The width of trenches and wheel tracks is ≈20 cm and of the RAT holes is ≈5 cm. The labeled traverse maps are from *Arvidson et al.* [2006]. True color images courtesy of NASA/JPL/Cornell as posted at http://marswatch.astro.cornell.edu/pancam_instrument/true_color.html, and other images as posted at http://marswatch.astro.cornell.edu/pancam_instrument/mosaics.html. *Bell et al.* [2003], *Bell et al.* [2006a], and *Bell et al.* [2006b] describe the image processing techniques and Pancam instrumentation in detail. The images in sol order are as follows: (a) Approximate true color mosaic of the "Road Cut" trench in the "Laguna Hollow" area on sol 47. (b) True color image of "Humphrey" following abrasion with the RAT (sequence P2597 sol 60). Humphrey is ≈60 cm tall. (c) Approximate true color mosaic of the "Big Hole" trench in typical soil on sol 116. (d) Approximate true color mosaic of the "Boroughs" trench in typical soil on sol 142. Boroughs is ≈11 cm deep. (e) True color image of "Wishstone" (sequence P2571 sol 342). Note wheel tracks for scale.

thickness locally exceeding ≈1 m [*Soderblom et al.*, 2004], overlying sulfate-rich sedimentary bedrock [e.g., *Grotzinger et al.*, 2005; *Jolliff and McLennan*, 2006; *McLennan et al.*, 2005; *Squyres et al.*, 2006b]. Therefore the soil and bedrock can each be deeper than the tens of centimeter GS sampling depths, sometimes acting as a semi-infinite layer and sometimes not, complicating the analysis. However, bedrock exposures are sparse along the rover traverse and limited largely to craters (e.g., Victoria) and fractures (e.g., Anatolia) [*Squyres et al.*, 2004a, 2006c].

[47] With the exception of a lag deposit of hematite spherules derived mostly from the bedrock, the soil is predominantly basaltic sand of potentially external origin [*Squyres et al.*, 2004a; *Weitz et al.*, 2006; *Soderblom et al.*,

Table 2. Identification Information of APXS Samples at Both MER Locations[a]

Rover	Sol	Sample Type	Integration Time, h	Target Name
Opportunity	81	T soil	4.0	BeagleBurrow_Trench
Opportunity	368	T soil	3.0	Left_of_peanut_TrenchFloor
Spirit	49	T hollows soil	6.5	Road Cut_Floor3
Spirit	50	T hollows soil	7.6	Road Cut_WallMIonl
Spirit	60	R unaltered rock	5.0	Humphrey_RAT2
Spirit	114	T typical soil	9.9	Bighole_RS2
Spirit	115	T typical soil	4.0	Bighole_Trico
Spirit	140	T typical soil	8.3	Boroughs_Mills_bottom
Spirit	141	T typical soil	4.0	Boroughs_Hellskitchen_side
Spirit	335	R altered rock	3.3	Wishstone_chisel_RAT

[a]Extracted from the work of *Gellert et al.* [2006] for Spirit and http://pds-geosciences.wustl.edu/geodata/mer1_mer2-m-apxs-5-oxide-sci-v1/merap_2xxx/data/apxs_oxides_mer1.csv for Opportunity. "R" refers to abrasion with the RAT, while "T" refers to excavation with the wheels. Sols are subsequent to landing at each site.

2004]. Furthermore, $w(H_2O)$ may be elevated in Meridiani outcrops (with a modeled maximum of ≈22%) due to hydrated sulfate minerals, while it is probably less than 4% in the soil [*Clark et al.*, 2005]. If applicable at GS footprint scales, this would attribute much of the GS-derived H content to the outcrop rather than the soil. Furthermore, with the exception of basaltic sands, the unique minerals at Meridiani may make the densities of its regolith components differ significantly from density estimates based on Viking observations (R. Sullivan, personal communication, 2005).

[48] Such issues considerably weaken the relevance of equations (1) and (4) in estimating a representative composition at Meridiani. However, as a first-order approximation to the representative Meridiani composition, we use equation (1) assuming a rock-free surface (i.e., $A_r = 0$) dominated by the (hematite-free) basaltic component of the soil material. Even though the areal fraction of soil as determined with IRTM data is not 100% (Table 1), it is sufficiently close to unity for our first-order approximation. As at Gusev, the areally dominant soil component (in the context of the GS sampling depths) was sampled by trenching experiments which also revealed the presence of finer grains at depth in addition to the volumetrically abundant basaltic grains [*Weitz et al.*, 2006; *Sullivan et al.*, 2005]. We represent this soil with the arithmetic mean (refer to equation (2) and related text for uncertainty estimation) composition at depth in two trenches, "BeagleBurrow_Trench" and "Left_of_peanut_TrenchFloor" (Figure 2 and Table 2). As evident in the low areal fractions of hematite and jarosite [*Klingelhöfer et al.*, 2004; *Morris et al.*, 2006b], these two trenches effectively exclude the lag deposit and other contributions from the outcrop unlike those from sols 25 ("Trench_floor") and 26 ("Trench_sidewall"). We use the recalibrated APXS-derived mass fractions (available at http://pds-geosciences.wustl.edu/geodata/mer1_mer2-m-apxs-5-oxide-sci-v1/merap_2xxx/data/apxs_oxides_mer1.csv) as an update to those given by *Rieder et al.* [2004].

[49] Complicating matters further, outcrop sampled in the current km scale traverse of Opportunity may not be representative of bedrock in the greater Sinus Meridiani region [e.g., *Edgett*, 2005] and by extension, within the GS's ≈440 km instrumental and ≈1800 km filter footprints. In addition, accurately modeling the compositional effect from rocks would require a checkerboard surface model, given the distinctly layered nature to the regolith at Meridiani. Such a model would consist strictly of weighting by the areal fractions of outcrop and soil without the use of bulk densities, since each layer would usually appear infinitely thick to the GS. However, a checkerboard model is unlikely to significantly improve the accuracy or precision of our calculated composition in the context of GS comparisons, particularly since the variability in soil depth is poorly known.

6.4. Pathfinder and the GS Normalization

[50] The reported geochemistry of rock and soil material at Pathfinder shows less heterogeneity than those at either Gusev or Meridiani. In part this may be due to the short Pathfinder traverse of about 100 m (since Sojourner rover remained within ≈10 m of the lander throughout the mission) [*Golombek et al.*, 1999] relative to MER's km scale traverse. Pathfinder also lacked the capability to brush rock surfaces or abrade them, as the MER rovers have done with the RAT, which may have potentially concealed compositional variations. For example, complex alteration processes have produced both brushable surface accumulations and abradable alteration zones on rocks at both MER sites [e.g., *Hurowitz et al.*, 2006], the compositional effects of which cannot be removed by the S extrapolation method used at Pathfinder [*Wänke et al.*, 2001].

[51] More important, the Pathfinder landing ellipse in Ares Vallis is larger [*Golombek et al.*, 1997] than those of either MER [*Arvidson et al.*, 2003; *Cabrol et al.*, 2003; *Golombek et al.*, 2003]. While the landing ellipse is an engineering constraint, missions with smaller landing ellipses are capable of reaching landing sites that are geologically homogeneous over smaller scales. Consequently, the much larger Pathfinder landing ellipse (located in a region less diverse than either MER site) and its immediate neighborhood present a geologically less heterogeneous area that is better suited for comparison with the GS given its coarse spatial resolution. Ironically, the advantage offered by the MER mission with smaller landing ellipses is lost to the GS since both ellipses were chosen to lie within geologically heterogeneous regions at GS footprint scales. For example, much as Lunokhod-2 was the first rover to traverse a geologic contact on the moon [e.g., *Basilevsky et al.*, 1977; *Basilevsky and Linkin*, 1996], Spirit is the first

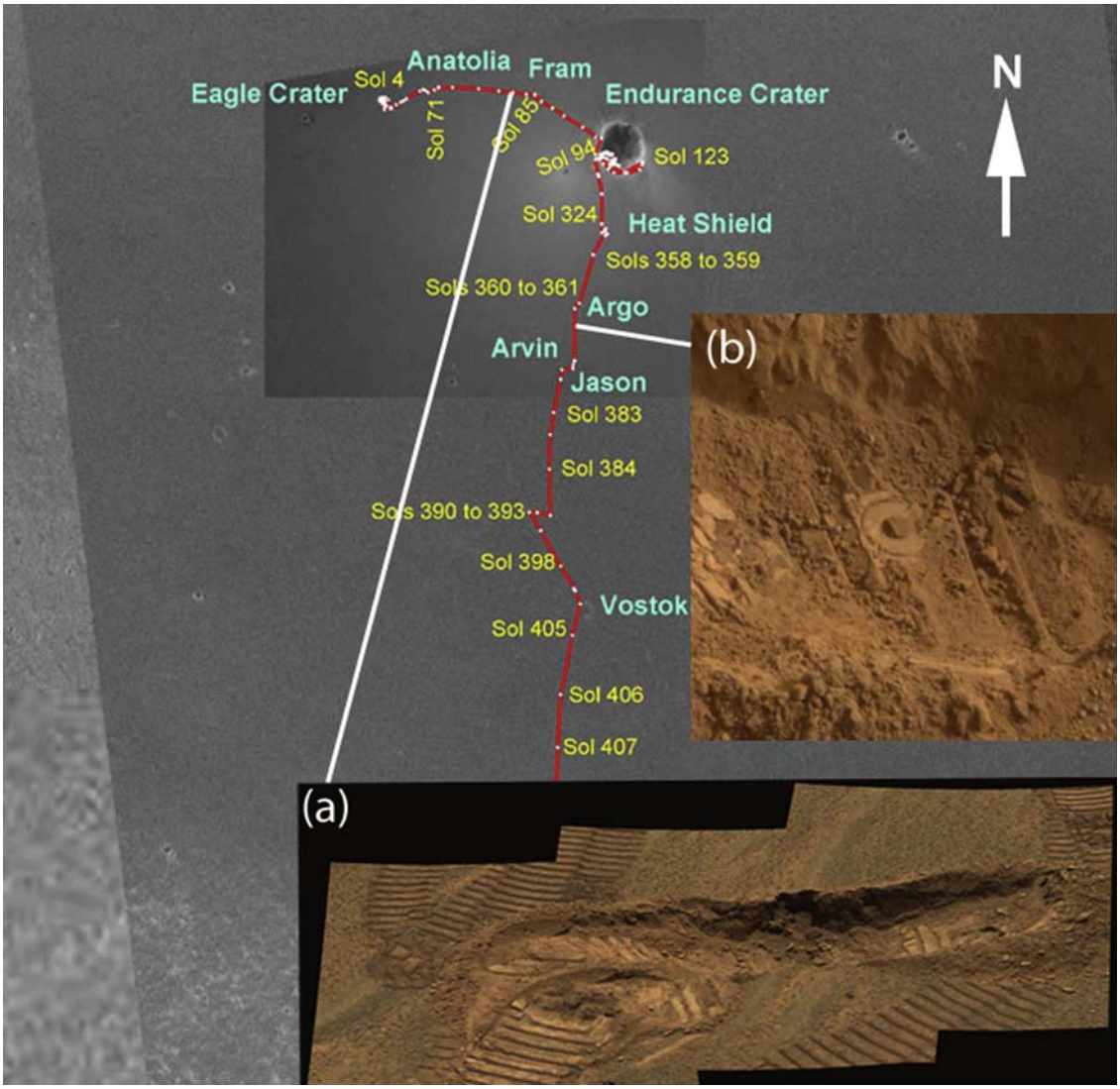

Figure 2. Images of trenches at Meridiani that were used to obtain APXS data for our study as traverse map insets. The width of each trench is ≈20 cm. The labeled traverse map is courtesy of NASA/JPL/OSU as posted at http://marsrovers.nasa.gov/mission/tm-opportunity/images/MERB_481_br2.jpg. *Bell et al.* [2003], *Bell et al.* [2006a], and *Bell et al.* [2006b] describe the image processing techniques and Pancam instrumentation in detail. (a) Approximate true color mosaic of the sol 81 ''BeagleBurrow_Trench'' area. The trench is ≈11 cm deep. Image courtesy of NASA/JPL-Caltech as posted at http://marsrovers.jpl.nasa.gov/gallery/press/opportunity/20040428a/09-SM-02-TrenchPan-B093R1.jpg. (b) Part of the sol 368 ''Left_of_peanut_TrenchFloor'' area in true color showing a Mössbauer imprint within. Image courtesy of NASA/JPL/Cornell as posted at http://marswatch.astro.cornell.edu/pancam_instrument/images/True/Sol373B_P2552_1_True_RAD.jpg.

rover to traverse a geologic contact on another planet [e.g., *Arvidson et al.*, 2006; *Crumpler et al.*, 2005].

[52] The apparent compositional homogeneity at Pathfinder enables us to use revised values for all samples, as reported by *Wänke et al.* [2001], to estimate the mean compositions of soil and rocks. *Brückner et al.* [2003] provide details of the refined calibration that was used by *Wänke et al.* [2001]. Data from both these papers are essentially in agreement. *Foley et al.* [2003] describe Pathfinder APXS data that were derived from an independent calibration and are very similar to those quoted by *Wänke et al.* [2001] and *Brückner et al.* [2003] for the major elements, while discrepancies exist for minor elements.

[53] The representative composition at Pathfinder estimated from the work of *Foley et al.* [2003] is (50 ± 20) % higher for Cl and (30 ± 10) % lower for K than that based on values by *Wänke et al.* [2001]. In spite of this, since all three works overlap within net uncertainties for the major elements Fe and Si, we do not anticipate significant changes to GS estimates should the data by *Foley et al.* [2003] be used. The Cr estimate has a minor caveat as well, since soil-free rock has been modeled without Cr [e.g., *Brückner et al.*, 2003; *Foley et al.*, 2003; *Wänke et al.*, 2001]. As a

Table 3. Calculated Representative in Situ Mass Fractions and Their GS-Derived Counterparts at Four Landing Sites[a]

Element	Opportunity	Pathfinder	SpiritH	SpiritHW	Viking 1
Al	4.69(0.23)	4.5(0.3)	4.38(0.17)	4.6(0.3)	4.4(1.1)
Ca	4.53(0.03)	4.8(0.4)	3.99(0.16)	4.07(0.22)	4.6(0.6)
Cl	0.466(0.006)	0.49(0.07)	0.71(0.08)	0.72(0.07)	0.71(0.17)
GS-derived Cl	0.59(0.06)	0.37(0.04)	0.68(0.06)		0.37(0.04)
Cr	0.303(0.007)	0.16(0.08)	0.26(0.02)	0.23(0.02)	-
Fe	13.8(0.7)	14.6(0.9)	12.3(0.3)	11.8(0.3)	13.2(1.3)
GS-derived Fe	15.4(1.3)	17.3(1.3)	15.7(1.2)		15.4(1.2)
GS-derived H_2O	5.4(0.6)	2.9(0.5)	7.4(0.6)		2.6(0.4)
K	0.336(0.016)	0.63(0.07)	0.25(0.02)	0.284(0.014)	0.22(0.13)
GS-derived K	0.316(0.023)	0.43(0.03)	0.328(0.020)		0.31(0.03)
Mg	4.18(0.13)	4.2(0.6)	5.36(0.18)	5.02(0.24)	3.3(0.6)
Mn	0.273(0.011)	0.40(0.08)	0.252(0.008)	0.238(0.006)	-
Na	1.58(0.05)	1.0(0.3)	1.70(0.03)	1.88(0.16)	-
P	0.32(0.02)	0.42(0.07)	0.295(0.010)	0.49(0.15)	-
S	2.1(0.4)	2.2(0.5)	3.4(0.5)	3.4(0.5)	2.7(0.7)
Si	20.2(0.6)	21.0(1.9)	18.5(0.5)	18.4(0.5)	22.6(1.6)
GS-derived Si	19.8(0.5)	21.0(0.5)	19.6(0.5)		20.9(0.5)
Ti	0.677(0.017)	0.55(0.10)	0.469(0.016)	0.59(0.08)	0.41(0.05)

[a]GS derivations are from Boynton et al. (submitted manuscript, 2006). Mass fractions are in %. The net uncertainty of each mass fraction is given parenthetically to one standard error ($1s_m$). Equation (2) and related text describe the uncertainty estimation for calculated in situ mass fractions, while Boynton et al. (submitted manuscript, 2006) describe that for GS-derived concentrations. SpiritHW uses an area-weighted mean of Humphrey and Wishstone compositions, while SpiritH only uses the composition of Humphrey. Note that only four of the elements have both representative in situ and GS-derived concentrations. Similarly, the GS-derived w(H) at each landing site, expressed as the stoichiometrically equivalent $w(H_2O)$ (C_{GS} in equation (4)), does not have an in situ counterpart.

result, our estimate of Cr assumes a modeled zero content of Cr in rocks, with only the uncertainty of w(Cr) in soil incorporated into equation (2).

7. Sensitivity of Representative Compositions to Unknowns

[54] The accuracy and precision of representative compositions are important considerations given the limited spatial sampling of in situ instruments, IRTM modeling of rock areal fractions, and Viking density estimates. As expected, the content of major elements, such as Si, is consistent across the landing sites and APXS measurements have rigorously quantified uncertainties. Rock areal fraction estimates from rovers and landers have been consistent with IRTM modeling as well. In addition, the density estimates are based upon reasonable parallels with terrestrial material. Collectively, these suggest that the representative compositions are sufficiently accurate for use at GS footprint scales and sampling depths, barring unknown systematic errors in instrument calibrations.

[55] However, there is some variability in rock abundance due to the massive difference in sampling area between the surface instruments and GS. Density uncertainties are poorly constrained, since none of the missions had the means to determine densities. An additional uncertainty is introduced by the oxidation state of Fe, though again, a reasonable value was used in our calculations. A final uncertainty affecting the Gusev representative composition is the areal ratio of typical soil to hollows soil. We estimated the effects of these uncertainties by varying rock abundance, rock density, and soil density values by 50%; varying the Fe oxidation state as +2, +2.5, and +3; and using a typical soil to hollows soil areal fraction ratio of 3 to 7. The alternative typical soil to hollows soil ratio was selected as a potential value at GS footprint scale, which is much larger than the Gusev crater, as well as to investigate compositional effects if hollows were to be areally dominant.

[56] The effect of the Fe oxidation state was minimal, changing the representative composition by less than 1%. Rock areal fraction and density variations caused representative compositions to vary by less than 7% at most. While affecting only the Gusev representative composition the last issue, areal fraction ratio of typical soil to hollows soil, altered the S content by as much as 26%, even though Si varied by only 6%. This was a consequence of the elevated S levels at mid-depth in the Boroughs trench wall [e.g., *Wang et al.*, 2006]. In summary, therefore, with the exception of Gusev, poorly constrained parameters in the representative composition calculation are unlikely to cause more than a 10% relative uncertainty. While Gusev may be subject to a higher uncertainty, major elements such as Si are still unlikely to vary by more than 15%. We report standard errors (computed with equation (2)) in Table 3 to one significant figure with the exception of those with 1 or 2 as the leading digit where we report to two significant figures. We accordingly retain the last significant figure of the result to be of the same order of magnitude as the uncertainty [e.g., *Taylor*, 1982, pp. 15–21].

8. Discussion of Results

[57] The representative in situ compositions as computed above are listed in Table 3. As evident in Figure 3, the concentrations of major elements vary less and have smaller relative uncertainties than those of many minor elements. Consider for example the difference in variability and uncertainty between K (dynamic range approximately a factor of 3) and Si (dynamic range approximately a factor of 1.2). Furthermore, the variability of K as represented by the standard deviation of the mass fractions is 49% of the (arithmetic) mean w(K) of all landing sites, while the variability is only 9% for Si and Fe. The similarity in major

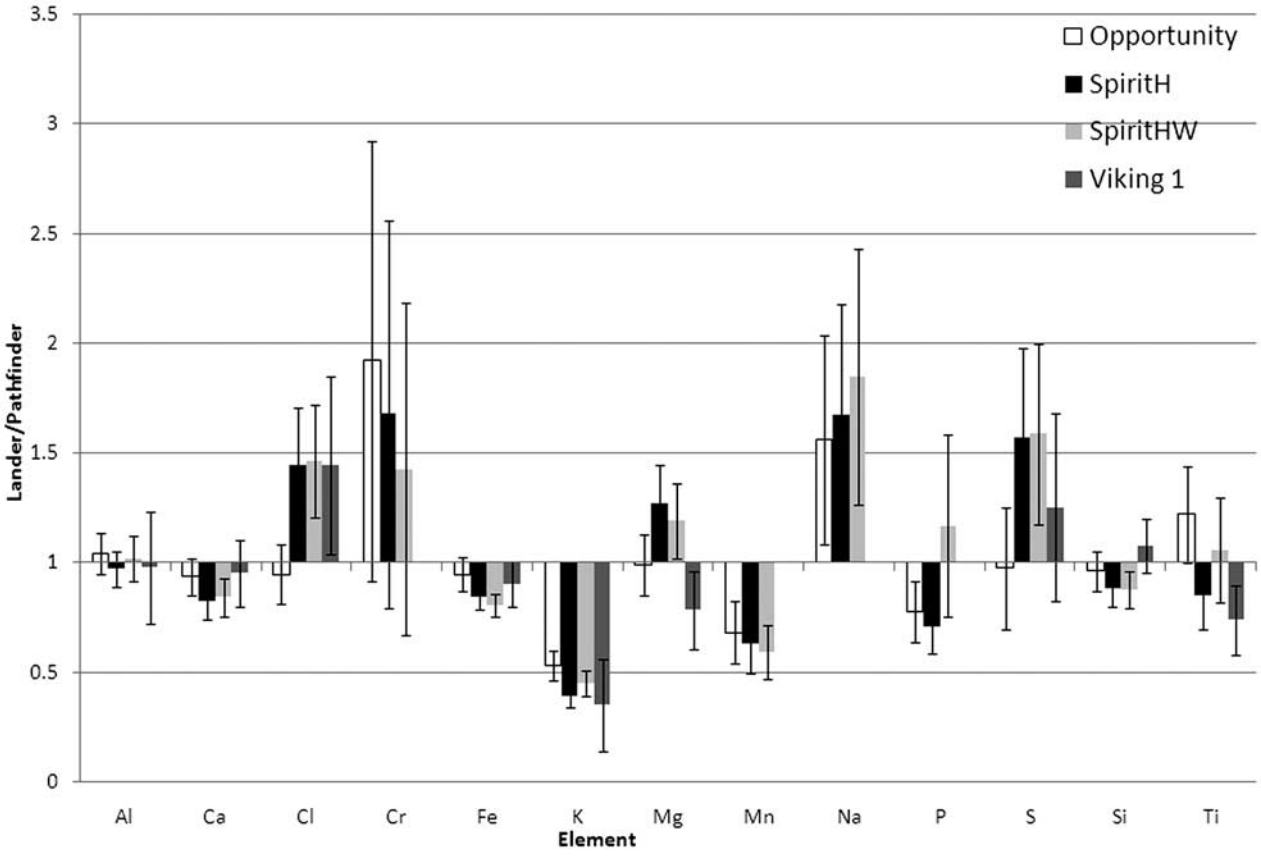

Figure 3. The variation in chemistry across the landing sites as the ratio of the chemical composition at each site to that at the Pathfinder site (data from Table 3). Deviation of the ratio from unity reflects differences with the Pathfinder composition. Error bars represent the standard error, $1s_m$, of the ratio as obtained by substituting the ratio for f in equation (2). The text related to equation (2) identifies the uncertainties that have been included in the error propagation. Note that Cr, Mn, Na, and P data are unavailable for Viking 1. SpiritHW uses an area-weighted mean of Humphrey and Wishstone compositions, while SpiritH only uses the composition of Humphrey.

elements across the four sites suggests that normalizing w(Si) to Pathfinder is unlikely to introduce systematic errors. On the other hand, normalization of minor elements to in situ values would have been more prone to error, given the variability and associated uncertainties of their mass fractions across the landing sites. The geochemical implications of representative in situ compositions, particularly in terms of their comparison with GS data, are discussed by *Karunatillake et al.* [2006], *Keller et al.* [2006b], *Newsom et al.* [2007], *Taylor et al.* [2006a], *Taylor et al.* [2006b], and Boynton et al. (submitted manuscript, 2006).

[58] Comparison of the two representative in situ compositions estimated for Gusev, as described in section 6.2, provides insight into the impact on the representative composition from the compositional variability of different rock types at a single landing site. That the impact is minor is evident in Figure 3, where the representative concentrations of most elements are similar even though Humphrey and Wishstone are compositionally distinct even with respect to major elements such as Fe [e.g., *Gellert et al.*, 2006]. The primary reason for the subdued effect is the areal dominance of the soil component which, due to the general absence of striking differences in soil composition between the plains and Columbia hills [e.g., *Arvidson et al.*, 2006], was taken to be compositionally uniform both within and beyond Gusev crater. Since the soil component is areally dominant across much of Mars [e.g., *Newsom et al.*, 2007; *Karunatillake et al.*, 2006], the GS should also be more sensitive to compositional variations of the Martian soils than of rocks. GS data indicate significant chemical variations in soil [*Newsom et al.*, 2007] in spite of evidence for compositionally similar soils across landing sites [e.g., *Yen et al.*, 2005].

[59] The GS-determined K content at Pathfinder is higher at the $1s_m$ level relative to the K content at the other sites, though not at the $2s_m$ level (Table 3). Si does not appear enriched at Pathfinder even at $1s_m$ (Table 3), which is consistent with the absence of Si enrichment in surface type 2 material [*Karunatillake et al.*, 2006]. The GS estimates are compared with the representative in situ estimates in Figure 4. In addition to the Si mass fractions, which approximate in situ values by virtue of the normalization, Cl and K also compare favorably. The favorable comparison for Cl (which overlaps with the GS value within $2s_m$) lends additional support for the Si normalization (Boynton et al., submitted manuscript, 2006). The

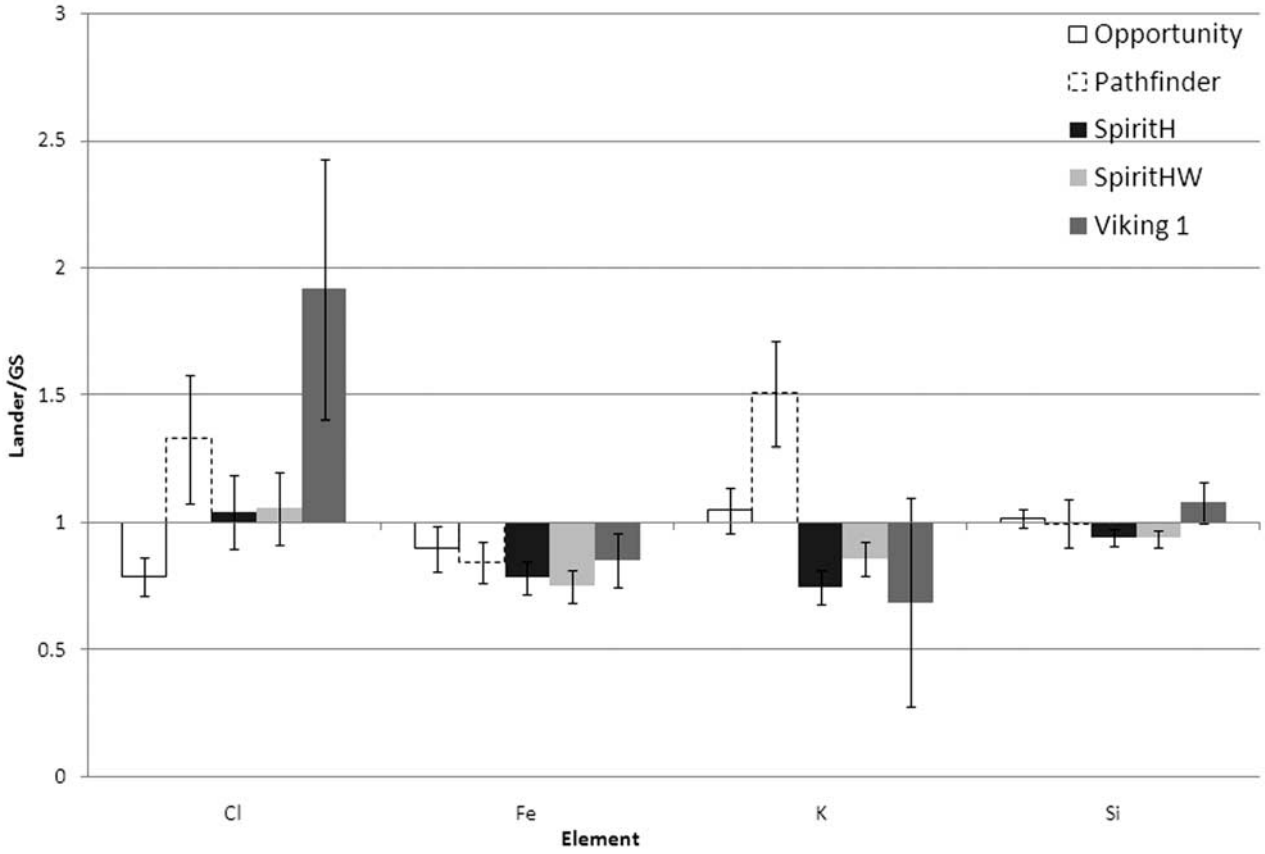

Figure 4. Representative in situ compositions compared with corresponding GS estimates for the four elements observed in common (Table 3) as the ratio of the calculated in situ value to the GS estimate at each landing site. Interpretation as in Figure 3. Note that the Si ratio for Pathfinder is unity by virtue of the GS normalization.

favorable comparison for K (for which the GS and in situ values overlap within $1s_m$ at Opportunity and Viking) is specially significant, since K is a radiogenic element unaffected by capture and scatter processes.

[60] However, the GS estimate of Fe content appears to be consistently higher, even though the relative difference, varying from a low of 10% at Meridiani to a high of 20% at Gusev, is always less than $3s_m$. Since the disparity exists across all landing sites in the same direction, it is unlikely to be an effect of the simplifications and sample selections we made in calculating representative in situ compositions at the four sites. Boynton et al. (submitted manuscript, 2006) discuss the implications of these comparisons in depth.

9. Conclusions

[61] Our study estimating the representative in situ compositions at four landing sites is an example of the synergy between remote sensing and surface missions [cf. *Bibring et al.*, 2006a]. For example, the GS determination of H and IRTM determination of rock abundance can be combined with surface data to derive representative in situ chemical compositions across large areas even though data from surface instruments are inherently local in scope. This method of estimating representative compositions at landing sites is applicable to future remote sensing missions as well. In addition, the representative in situ compositions that we derive (Table 3) may be used in the normalization and "ground truth" comparisons of future remote sensing missions that have depth and lateral spatial resolutions comparable to the GS. As expected at such spatial scales the concentration of major elements tends to be similar across landing sites. However, the compositional diversity evident at the MER sites should be utilized for remote sensing missions with finer lateral spatial resolution.

[62] Future constraints on Martian regolith mechanical properties would help increase the precision of our estimates, since bulk density uncertainties (refer to section 4) dominate the standard errors in Table 3. Furthermore, as revealed by the extreme cases in section 7 and given the areal dominance of soil, better constrained densities and areal fractions of regolith components, not elemental oxidation states, would enhance the accuracy of our calculations. In this respect, the future availability of high resolution images and spectral data (such as the Mars Reconnaissance Orbiter data) for the different landing sites would be very useful, since it would greatly enhance the estimates of relative amounts of different regolith components over the entire GS footprint at each landing site. In addition, improved remote sensing data may help reveal and establish the GS footprint most representative of a given landing site, even when it is not centered at the site

coordinates. Such improvements would be further enhanced by more realistic modeling of material mixing geometries [e.g., *Kim et al.*, 2006a] by revealing the compositional effect of rocks in spite of their low areal abundance. Better constraints on the surface GCR flux with the Mars Science Laboratory Radiation Assessment Detector [*Hassler et al.*, 2006; *Cucinotta et al.*, 2007] may help refine the GS forward modeling as well.

[63] **Acknowledgments.** We thank the Mars Odyssey Project for support. Robert Sullivan was instrumental in preventing a simplistic treatment of regolith properties at the two MER sites and in ensuring that we selected the appropriate surface samples for comparison with the GS data sets. We are grateful for the time and effort he spent in aiding us. James Dohm advised us on geological properties, while Phillip R. Christensen provided Viking IRTM data. We also thank Jeff Taylor for identifying important caveats to the compositional results presented here and helping us better articulate those limitations. Our reviewers helped refine the presentation in general and discussion of uncertainties in particular.

References

Anderson, D. M., and A. R. Tice (1979), The analysis of water in the Martian regolith, *J. Mol. Evol.*, *14*, 33–38, doi:10.1007/BF01732365.

Arvidson, R. E., F. P. Seelos IV, K. S. Deal, W. C. Koeppen, N. O. Snider, J. M. Kieniewicz, B. M. Hynek, M. T. Mellon, and J. B. Garvin (2003), Mantled and exhumed terrains in Terra Meridiani, Mars, *J. Geophys. Res.*, *108*(E12), 8073, doi:10.1029/2002JE001982.

Arvidson, R. E., et al. (2004a), Localization and physical properties experiments conducted by Spirit at Gusev crater, *Science*, *305*(5685), 821–824, doi:10.1126/science.1099922.

Arvidson, R. E., et al. (2004b), Localization and physical property experiments conducted by Opportunity at Meridiani Planum, *Science*, *306*(5702), 1730–1733, doi:10.1126/science.1104211.

Arvidson, R. E., et al. (2006), Overview of the Spirit Mars Exploration Rover Mission to Gusev Crater: Landing site to Backstay Rock in the Columbia Hills, *J. Geophys. Res.*, *111*, E02S01, doi:10.1029/2005JE002499.

Banin, A., B. C. Clark, and H. Wänke (1992), Surface chemistry and mineralogy, in *Mars*, edited by H. H. Kieffer, chap. 18, pp. 594–625, Univ. of Ariz. Press, Tucson.

Basilevsky, A. T., and V. M. Linkin (1996), Lunar rover sample return: Lunokhod/Luna heritage and perspectives, *Adv. Space Res.*, *18*(11), 83–83, doi:10.1016/0273-1177(96)00106-8.

Basilevsky, A. T., C. P. Florensky, and L. B. Ronca (1977), Possible lunar outcrop—Study of lunokhod-2 data, *Moon*, *17*(1), 19–28, doi:10.1007/BF00566850.

Bell, J. F., III, et al. (2003), Mars Exploration Rover Athena Panoramic Camera (Pancam) investigation, *J. Geophys. Res.*, *108*(E12), 8063, doi:10.1029/2003JE002070.

Bell, J. F., et al. (2004), Pancam multispectral imaging results from the Opportunity Rover at Meridiani planum, *Science*, *306*, 1703–1709, doi:10.1126/science.1105245.

Bell, J. F., III, J. Joseph, J. N. Sohl-Dickstein, H. M. Arneson, M. J. Johnson, M. T. Lemmon, and D. Savransky (2006a), In-flight calibration and performance of the Mars Exploration Rover Panoramic Camera (Pancam) instruments, *J. Geophys. Res.*, *111*, E02S03, doi:10.1029/2005JE002444.

Bell, J. F., III, D. Savransky, and M. J. Wolff (2006b), Chromaticity of the Martian sky as observed by the Mars Exploration Rover Pancam instruments, *J. Geophys. Res.*, *111*, E12S05, doi:10.1029/2006JE002687.

Bibring, J. P., S. W. Squyres, and R. E. Arvidson (2006a), Merging views on Mars, *Science*, *313*(5795), 1899–1901, doi:10.1126/science.1132311.

Bibring, J. P., et al. (2006b), Global mineralogical and aqueous Mars history derived from OMEGA/Mars Express data, *Science*, *312*(5772), 400–404, doi:10.1126/science.1122659.

Boynton, W. V., et al. (2004), The Mars Odyssey Gamma-Ray Spectrometer instrument suite, *Space Sci. Rev.*, *110*(1–2), 37–83, doi:10.1023/B:SPAC.0000021007.76126.15.

Brückner, J., G. Dreibus, R. Rieder, and H. Wänke (2003), Refined data of Alpha Proton X-ray Spectrometer analyses of soils and rocks at the Mars Pathfinder site: Implications for surface chemistry, *J. Geophys. Res.*, *108*(E12), 8094, doi:10.1029/2003JE002060.

Cabrol, N. A., et al. (2003), Exploring Gusev Crater with Spirit: Review of science objectives and testable hypotheses, *J. Geophys. Res.*, *108*(E12), 8076, doi:10.1029/2002JE002026.

Cabrol, N. A., J. D. Farmer, E. A. Grin, L. Richter, L. Soderblom, R. Li, K. Herkenhoff, G. A. Landis, and R. E. Arvidson (2006), Aqueous processes at Gusev crater inferred from physical properties of rocks and soils along the Spirit traverse, *J. Geophys. Res.*, *111*, E02S20, doi:10.1029/2005JE002490.

Christensen, P. R. (1986), The spatial distribution of rocks on Mars, *Icarus*, *68*(2), 217–238, doi:10.1016/0019-1035 (86)90020-5.

Clark, B. C., III, et al. (1977), The Viking X-ray fluorescence experiment: Analytical methods and early results, *J. Geophys. Res.*, *82*, 4577–4594.

Clark, B. C., A. K. Baird, R. J. Weldon, D. M. Tsusaki, L. Schnabel, and M. P. Candelaria (1982), Chemical composition of Martian fines, *J. Geophys. Res.*, *87*, 10,059–10,067.

Clark, B. C., et al. (2005), Chemistry and mineralogy of outcrops at Meridiani Planum, *Earth Planet. Sci. Lett.*, *240*(1), 73–94, doi:10.1016/j.epsl.2005.09.040.

Crumpler, L. S., et al. (2005), Mars Exploration Rover Geologic traverse by the Spirit rover in the Plains of Gusev Crater, Mars, *Geology*, *33*(10), 809–812, doi:10.1130/G21673.1.

Cucinotta, F. A., M.-H. Kim, S. I. Schneider, and D. M. Hassler (2007), Description of light ion production cross sections and fluxes on the Mars surface using the QMSFRG model, in *Proceedings of the 4th IWSRR*, *Radiat. Environ. Biophys.*, *46*, 101–106, doi:10.1007/s00411-007-0099-y.

Edgett, K. S. (2005), The sedimentary rocks of Sinus Meridiani: Five key observations from data acquired by the Mars Global Surveyor and Mars Odyssey orbiters, *Mars*, *1*, 5–58, doi:10.1555/mars.2005.0002.

Evans, L. G., R. C. Reedy, R. D. Starr, K. E. Kerry, and W. V. Boynton (2006), Analysis of gamma ray spectra measured by Mars Odyssey, *J. Geophys. Res.*, *111*, E03S04, doi:10.1029/2005JE002657 [printed *112*(E3), 2007].

Farrand, W. H., J. F. Bell III, J. R. Johnson, S. W. Squyres, J. Soderblom, and D. W. Ming (2006), Spectral variability among rocks in visible and near-infrared multispectral Pancam data collected at Gusev crater: Examinations using spectral mixture analysis and related techniques, *J. Geophys. Res.*, *111*, E02S15, doi:10.1029/2005JE002495.

Fergason, R. L., P. R. Christensen, J. F. Bell III, M. P. Golombek, K. E. Herkenhoff, and H. H. Kieffer (2006), Physical properties of the Mars Exploration Rover landing sites as inferred from Mini-TES-derived thermal inertia, *J. Geophys. Res.*, *111*, E02S21, doi:10.1029/2005JE002583.

Foley, C. N., T. Economou, and R. N. Clayton (2003), Final chemical results from the Mars Pathfinder alpha proton X-ray spectrometer, *J. Geophys. Res.*, *108*(E12), 8096, doi:10.1029/2002JE002019.

Gellert, R., et al. (2004), Chemistry of rocks and soils in Gusev Crater from the Alpha Particle X-ray Spectrometer, *Science*, *305*(5685), 829–832, doi:10.1126/science.1099913.

Gellert, R., et al. (2006), Alpha Particle X-Ray Spectrometer (APXS): Results from Gusev crater and calibration report, *J. Geophys. Res.*, *111*, E02S05, doi:10.1029/2005JE002555.

Golombek, M. P., R. A. Cook, H. J. Moore, and T. J. Parker (1997), Selection of the Mars Pathfinder landing site, *J. Geophys. Res.*, *102*(E2), 3967–3988.

Golombek, M. P., et al. (1999), Overview of the Mars Pathfinder mission: Launch through landing, surface operations, data sets, and science results, *J. Geophys. Res.*, *104*(E4), 8523–8554.

Golombek, M. P., et al. (2003), Selection of the Mars Exploration Rover landing sites, *J. Geophys. Res.*, *108*(E12), 8072, doi:10.1029/2003JE002074.

Golombek, M. P., et al. (2005), Assessment of Mars Exploration Rover landing site predictions, *Nature*, *436*(7047), 44–48, doi:10.1038/nature03600.

Golombek, M. P., et al. (2006), Geology of the Gusev cratered plains from the Spirit rover transverse, *J. Geophys. Res.*, *111*, E02S07, doi:10.1029/2005JE002503.

Grant, J. A., et al. (2004), Surficial deposits at Gusev crater along Spirit rover traverses, *Science*, *305*(5685), 807–810, doi:10.1126/science.1099849.

Greeley, R., et al. (2005), Martian variable features: New insight from the Mars Express Orbiter and the Mars Exploration Rover Spirit, *J. Geophys. Res.*, *110*, E06002, doi:10.1029/2005JE002403.

Grotzinger, J. P., et al. (2005), Stratigraphy and sedimentology of a dry to wet eolian depositional system, Burns formation, Meridiani Planum, Mars, *Earth Planet. Sci. Lett.*, *240*(1), 11–72, doi:10.1016/j.epsl.2005.09.039.

Haining, R. (2003), *Spatial Data Analysis: Theory and Practice*, Cambridge University Press, New York.

Haskin, L. A., et al. (2005), Water alteration of rocks and soils on Mars at the Spirit rover site in Gusev crater, *Nature*, *436*(7047), 66–69, doi:10.1038/nature03640.

Hassler, D. M., et al. (2006), The radiation assessment detector (RAD) on the Mars Science Laboratory (MSL), paper presented at 36th COSPAR Scientific Assembly, Comm. on Space Res., Beijing.

Herkenhoff, K. E., et al. (2006), Overview of the Microscopic Imager Investigation during Spirit's first 450 sols in Gusev crater, *J. Geophys. Res.*, *111*, E02S04, doi:10.1029/2005JE002574.

Hurowitz, J. A., S. M. McLennan, N. J. Tosca, R. E. Arvidson, J. R. Michalski, D. W. Ming, C. Schröder, and S. W. Squyres (2006), In situ and experimental evidence for acidic weathering of rocks and soils on Mars, *J. Geophys. Res.*, *111*, E02S19, doi:10.1029/2005JE002515.

Jerolmack, D. J., D. Mohrig, J. P. Grotzinger, D. A. Fike, and W. A. Watters (2006), Spatial grain size sorting in eolian ripples and estimation of wind conditions on planetary surfaces: Application to Meridiani Planum, Mars, *J. Geophys. Res.*, *111*, E12S02, doi:10.1029/2005JE002544.

Jolliff, B. L., and S. M. McLennan (2006), Evidence for water at Meridiani, *Elements*, *2*, 163–167.

Karunatillake, S., et al. (2006), Composition of northern low-albedo regions of Mars: Insights from the Mars Odyssey Gamma Ray Spectrometer, *J. Geophys. Res.*, *111*, E03S05, doi:10.1029/2006JE002675 [printed *112*(E3), 2007].

Keller, J. M., W. V. Boynton, R. M. S. Williams, and S. Karunatillake (2006a), Analysis of layering at Mars near-surface using attenuation of chlorine gamma rays, *Proc. Lunar Planet. Sci. Conf. 37th*, *37th*, Abstract 2343.

Keller, J. M., et al. (2006b), Equatorial and midlatitude distribution of chlorine measured by Mars Odyssey GRS, *J. Geophys. Res.*, *111*, E03S08, doi:10.1029/2006JE002679 [printed *112*(E3), 2007].

Kim, K. J., W. V. Boynton, M. Finch, R. M. S. Williams, R. C. Reedy, and D. M. Drake (2006a), Effects of rocks on neutron and gamma-ray production in Martian surface soil, *Proc. Lunar Planet. Sci. Conf. 37th*, *37th*, Abstract 2356.

Kim, K. J., D. M. Drake, R. C. Reedy, R. M. S. Williams, and W. V. Boynton (2006b), Theoretical fluxes of gamma rays from the Martian surface, *J. Geophys. Res.*, *111*, E03S09, doi:10.1029/2005JE002655 [printed *112*(E3), 2007].

Klingelhöfer, G., et al. (2004), Jarosite and hematite at Meridiani Planum from Opportunity's Mössbauer Spectrometer, *Science*, *306*(5702), 1740–1745, doi:10.1126/science.1104653.

Kobayashi, M., et al. (2005), Germanium detector with Stirling cryocooler for lunar gamma-ray spectroscopy, *Nucl. Instrum. Methods Phys. Res., Sect. A*, *548*(3), 401–410, doi:10.1016/j.nima.2005.03.170.

Lane, M. D., J. L. Bishop, M. D. Dyar, M. Parente, P. L. King, and B. C. Hyde (2007), Identifying the phosphate and ferric sulfate minerals in the Paso Robles soils (Gusev crater, Mars) using an integrated spectral approach, *Lunar Planet. Sci.*, *XXXVIII*, Abstract 2176.

Loss, R. D. (2003), Atomic weights of the elements 2001 (IUPAC technical report), *Pure Appl. Chem.*, *75*(8), 1107–1122.

Mandel, J. (1964), *The Statistical Analysis of Experimental Data*, 410 pp., Interscience, New York.

Masarik, J., and R. C. Reedy (1996), Gamma ray production and transport in Mars, *J. Geophys. Res.*, *101*(E8), 18,891–18,912.

Mayo, A. P., W. T. Blackshear, R. H. Tolson, W. H. Michael, G. M. Kelly, J. P. Brenkle, and T. A. Komarek (1977), Lander locations, Mars physical ephemeris, and solar system parameters-determination from Viking lander tracking data, *J. Geophys. Res.*, *82*, 4297–4303.

McLennan, S. M., et al. (2005), Provenance and diagenesis of the evaporite–bearing Burns formation, Meridiani Planum, Mars, *Earth Planet. Sci. Lett.*, *240*(1), 95–121, doi:10.1016/j.epsl.2005.09.041.

McNutt, J., L. Ralph, S. C. Solomon, R. E. Gold, J. C. Leary, and the MESSENGER Team (2006), The MESSENGER mission to Mercury: Development history and early mission status, *Adv. Space Res.*, *38*(4), 564–571, doi:10.1016/j.asr.2005.05.044.

McSween, H. Y., Jr. (1994), What we have learned about Mars from SNC meteorites, *Meteoritics*, *29*, 757–779.

McSween, H. Y., Jr. (2002), The rocks of Mars, from far and near, *Meteorit. Planet. Sci.*, *37*(1), 7–25.

McSween, H. Y., Jr., and K. Keil (2000), Mixing relationships in the Martian regolith and the composition of globally homogeneous dust, *Geochim. Cosmochim. Acta*, *64*(12), 2155–2166, doi:10.1016/S0016-7037(99)00401-9.

McSween, H. Y., et al. (2004), Basaltic rocks analyzed by the Spirit rover in Gusev crater, *Science*, *305*(5685), 842–845, doi:10.1126/science.3050842.

Metzger, A. E., and D. M. Drake (1990), Identification of lunar rock types and search for polar ice by gamma ray spectroscopy, *J. Geophys. Res.*, *95*, 449–460.

Moore, H. J., and B. M. Jakosky (1989), Viking landing sites, remote-sensing observations, and physical properties of Martian surface materials, *Icarus*, *81*(1), 164–184, doi:10.1016/0019-1035(89)90132-2.

Moore, H. J., and J. Keller (1991), Surface-material maps of Viking landing sites on Mars, in *Planetary Geology and Geophysics Program Report*, vol. 2005, edited by T. A. Maxwell, pp. 160–162, NASA, Washington, D. C.

Moore, H. J., R. E. Hutton, R. F. Scott, C. R. Spitzer, and R. W. Shorthill (1977), Surface materials of Viking landing sites, *J. Geophys. Res.*, *82*, 4497–4523.

Morris, R. V., et al. (2004), Mineralogy at Gusev crater from the Mössbauer spectrometer on the Spirit Rover, *Science*, *305*(5685), 833–836, doi:10.1126/science.1100020.

Morris, R. V., et al. (2006a), Mössbauer mineralogy of rock, soil, and dust at Gusev crater, Mars: Spirit's journey through weakly altered olivine basalt on the plains and pervasively altered basalt in the Columbia Hills, *J. Geophys. Res.*, *111*, E02S13, doi:10.1029/2005JE002584.

Morris, R. V., et al. (2006b), Mössbauer mineralogy of rock, soil, and dust at Meridiani Planum, Mars: Opportunity's journey across sulfate-rich outcrop, basaltic sand and dust, and hematite lag deposits, *J. Geophys. Res.*, *111*, E12S15, doi:10.1029/2006JE002791.

Mustard, J. F., and C. D. Cooper (2005), Joint analysis of ISM and TES spectra: The utility of multiple wavelength regimes for Martian surface studies, *J. Geophys. Res.*, *110*, E05012, doi:10.1029/2004JE002355.

Newsom, H. E., et al. (2007), Geochemistry of Martian soil and bedrock in mantled and less mantled terrains with gamma ray data from Mars Odyssey, *J. Geophys. Res.*, *112*, E03S12, doi:10.1029/2006JE002680.

Olhoeft, G. R., and G. R. Johnson (1989), Densities of rocks and minerals, in *Practical Handbook of Physical Properties of Rocks and Minerals*, 1st ed., pp. 139–175, CRC Press, Boca Raton, Fla.

Pirard, B., C. d'Uston, S. Maurice, and O. Gasnault (2005), Performance limits on new generation scintillators for planetary gamma-ray spectroscopy, *Proc. Lunar Planet. Sci. Conf. 36th*, *36th*, Abstract 2187.

Rieder, R., H. Wänke, T. Economou, and A. Turkevich (1997), Determination of the chemical composition of Martian soil and rocks: The alpha proton X ray spectrometer, *J. Geophys. Res.*, *102*(E2), 4027–4044.

Rieder, R., R. Gellert, J. Brückner, G. Klingelhöfer, G. Dreibus, A. Yen, and S. W. Squyres (2003), The new Athena alpha particle X-ray spectrometer for the Mars Exploration Rovers, *J. Geophys. Res.*, *108*(E12), 8066, doi:10.1029/2003JE002150.

Rieder, R., et al. (2004), Chemistry of rocks and soils at Meridiani Planum from the Alpha Particle X–ray Spectrometer, *Science*, *306*(5702), 1746–1749, doi:10.1126/science.1104358.

Shkuratov, Y. G., V. G. Kaydash, D. G. Stankevich, L. V. Starukhina, P. C. Pinet, S. D. Chevrel, and Y. H. Daydou (2005), Derivation of elemental abundance maps at intermediate resolution from optical interpolation of lunar prospector gamma-ray spectrometer data, *Planet. Space Sci.*, *53*(12), 1287–1301, doi:10.1016/j.pss.2005.07.001.

Soderblom, L. A., et al. (2004), Soils of Eagle crater and Meridiani Planum at the Opportunity Rover landing site, *Science*, *306*(5702), 1723–1726, doi:10.1126/science.1105127.

Squyres, S. W., and L. G. Evans (1992), Effects of material mixing on planetary gamma-ray spectroscopy, *J. Geophys. Res.*, *97*(E9), 14,701–14,715.

Squyres, S. W., et al. (2004a), The Opportunity rover's Athena science investigation at Meridiani Planum, Mars, *Science*, *306*(5702), 1698–1703, doi:10.1126/science.1106171.

Squyres, S. W., et al. (2004b), The Spirit rover's Athena science investigation at Gusev Crater, Mars, *Science*, *305*(5685), 794–799, doi:10.1126/science.1100194.

Squyres, S. W., et al. (2006a), Rocks of the Columbia Hills, *J. Geophys. Res.*, *111*, E02S11, doi:10.1029/2005JE002562.

Squyres, S. W., et al. (2006b), Planetary science: Bedrock formation at Meridiani Planum, *Nature*, *443*(7107), E1–E2, doi:10.1038/nature05212.

Squyres, S. W., et al. (2006c), Two years at Meridiani Planum: Results from the Opportunity rover, *Science*, *313*(5792), 1403–1407, doi:10.1126/science.1130890.

Sullivan, R., et al. (2005), Aeolian processes at the Mars Exploration Rover Meridiani Planum landing site, *Nature*, *436*(7047), 58–61, doi:10.1038/nature03641.

Taylor, G. J., et al. (2006a), Variations in K/Th on Mars, *J. Geophys. Res.*, *111*, E03S06, doi:10.1029/2006JE002676 [printed *112*(E3), 2007].

Taylor, G. J., et al. (2006b), Bulk composition and early differentiation of Mars, *J. Geophys. Res.*, *111*, E03S10, doi:10.1029/2005JE002645 [printed *112*(E3), 2007].

Taylor, J. R. (1982), *An Introduction to Error Analysis*, 270 pp., Univ. Sci. Books, Herndon, Va.

Wang, A., et al. (2006), Sulfate deposition in subsurface regolith in Gusev crater, Mars, *J. Geophys. Res.*, *111*, E02S17, doi:10.1029/2005JE002513.

Wang, A., J. F. Bell, and R. Li (2007), Salty soils at Gusev crater as revealed by Mars Exploration Rover Spirit, *Lunar Planet. Sci.*, (XXXVIII), Abstract 1196.

Wänke, H., J. Brückner, G. Dreibus, R. Rieder, and I. Ryabchikov (2001), Chemical composition of rocks and soils at the Pathfinder site, *Space Sci. Rev.*, *96*(1–4), 317–330, doi:10.1023/A:1011961725645.

Weitz, C. M., R. C. Anderson, J. F. Bell III, W. H. Farrand, K. E. Herkenhoff, J. R. Johnson, B. L. Jolliff, R. V. Morris, S. W. Squyres, and R. J. Sullivan

(2006), Soil grain analyses at Meridiani Planum, Mars, *J. Geophys. Res.*, *111*, E12S04, doi:10.1029/2005JE002541.

Yen, A. S., et al. (2005), An integrated view of the chemistry and mineralogy of Martian soils, *Nature*, *436*(7047), 49–54, doi:10.1038/nature03637.

Young, H. D. (1962), *Statistical Treatment of Experimental Data*, 172 pp., McGraw-Hill, New York.

W. V. Boynton and D. M. Janes, Lunar and Planetary Laboratory, University of Arizona, 1629 East University Boulevard, Tucson, AZ 85721, USA.

J. Brückner, Abteilung Geochemie, Max-Planck-Institut für Chemie, Postfach 3060, D-55020 Mainz, Germany.

O. Gasnault, Centre d'Etude Spatiale des Rayonnements/Centre National de la Recherche Scientifique/Université Paul Sabatier Toulouse, 9 Avenue Colonel Roche, BP 4346, F-31028 Toulouse Cedex 4, France.

S. Karunatillake and S. W. Squyres, Department of Astronomy, Cornell University, 514 Space Sciences Building, Ithaca, NY 14853, USA. (wk43@cornell.edu)

J. M. Keller, Physics Department, California Polytechnic State University, San Luis Obispo, CA 93407, USA.

H. E. Newsom, Institute of Meteoritics and Department of Earth and Planetary Sciences, University of New Mexico, Room 306D, Northrop Hall, Albuquerque, NM 87131, USA.